

International Conference on Space Optics—ICSO 2018

Chania, Greece

9–12 October 2018

Edited by Zoran Sodnik, Nikos Karafolas, and Bruno Cugny



Ga-free InAs/InAsSb type-II superlattice (T2SL) photodetector for high operating temperature in the midwave infrared spectral domain

J. -P. Perez

Q. Durlin

P. Christol



Ga-free InAs/InAsSb type-II superlattice (T2SL) photodetector for High Operating Temperature in the midwave infrared spectral domain

J.P. Perez*^a, Q. Durlin^a, P. Christol^a

^aIES, Université de Montpellier, CNRS, F- 34000, Montpellier, France

ABSTRACT

We studied Ga-free InAs/InAsSb type-II superlattice (T2SL) in terms of period, thickness and antimony composition as a photon absorbing active layer (AL) of a suitable XBn structure for full mid-wavelength infrared domain (MWIR, 3-5 μ m) detection. The SL photodetector structures were fabricated by molecular beam epitaxy (MBE) on n-type GaSb substrate and exhibited cut-off wavelength between 5 μ m and 5.5 μ m at 150K. Electro-optical and electrical results of the device are reported and compared to the usual InSb MWIR photodiode.

Keywords: Infrared photodetector, type II superlattice, molecular beam epitaxy

1. INTRODUCTION

Recently, InAsSb-based XB_n photovoltaic devices (called *bariodes*¹) and lattice-matched to GaSb substrate have reached impressively low dark current allowing temperature operation as high as 150K and cut-off wavelength around 4.2 μ m. In this notation, "X" stands for the n- or p-type contact layer, "B", for the n-type, wide bandgap, barrier layer, and "n", for the n-type, narrow bandgap, active layer. Such IR photodetectors called HOT (High Operating Temperature) detectors have been developed to answer new needs like the compactness and the reduction of cryopower which are key features for the SWaP (Size Weight and Power) requirements². Nevertheless, only the [3-4.2 μ m] part of the MWIR [3-5 μ m] domain is addressed in that case.

Nevertheless, according to Planck's law and considering a blackbody at 300K without any IR system or transparency windows considerations, the power emitted per unit area at the surface of the blackbody in the [3-4.2 μ m] range represents only 18% of the total power in the [3-5 μ m] range. Therefore, taking into account the full MWIR transparency window would significantly improve the IR signal to noise ratio and finally the IR imaging performances³. Consequently, there is an obvious need to extend the operational wavelength of the XBn InAsSb HOT detector.

In that way, one can consider a type-II InAs/GaSb superlattice (T2SL) on GaSb substrate⁴. Unfortunately, such T2SL devices are penalized by a low minority carrier lifetime (around 100 ns in the MWIR) due to the presence of Ga-related native defects in the SL period⁵ leading typically to a temperature operation lower than 110K for a 5 μ m cut-off⁶. An extended cut-off was achieved recently by using an InAsSb bulk absorber material with a antimony content higher than the one lattice-matched to GaSb, leading to a cut-off wavelength higher than 5 μ m. This was possible using a 1.5 μ m thick AlSb buffer layer⁷. An alternative to the previously mentioned InAs/GaSb T2SL could be the Ga-free InAs/InAsSb T2SL highlighting carrier lifetime value as long as 9 μ s at 80K in the MWIR⁸. Moreover, results on first Ga-free T2SL MWIR detectors have recently been reported by US research groups^{9,10}. Therefore, the purpose of our work is to combine the XBn design with a Ga-free InAs/InAsSb SL absorbing layer.

In this paper, InAs/InAsSb SL grown by molecular beam epitaxy (MBE) is first studied. Choices of superlattice period and antimony composition (x_{Sb}) of the InAsSb ternary alloy to obtain high absorption in the full MWIR domain are presented. MBE growth conditions to achieve strain-balanced InAs/InAsSb SL structure on GaSb substrate are then detailed. Next, optical characterizations such as photoluminescence and minority carrier lifetime performed on dedicated structures are reported. Finally, we report electro-optical and electrical measurements of such Ga-free SL structure in XBn configuration.

2. CHOICE OF THE GA-FREE SL PERIOD

InAs/InAs_{1-x}Sb_x SL can be strained balanced on GaSb by setting the average lattice parameter of one period of the SL equal to the lattice parameter of GaSb. It follows that InAsSb and InAs layer thicknesses (t_{InAsSb} and t_{InAs}) as function of the antimony composition (x_{Sb}) and SL period (P) can be calculated by using Eqs(1) and (2):

$$t_{\text{InAsSb}} = \frac{a_{\text{GaSb}} - a_{\text{InAs}}}{a_{\text{InSb}} - a_{\text{InAs}}} \cdot \frac{P}{x_{\text{Sb}}} = 0.09 \cdot \frac{P}{x_{\text{Sb}}} \quad (1)$$

$$t_{\text{InAs}} + t_{\text{InAsSb}} = P \quad (2)$$

Where $a_{\text{GaSb}} = 6.0954 \text{ \AA}$; $a_{\text{InAs}} = 6.0584 \text{ \AA}$ and $a_{\text{InSb}} = 6.4794 \text{ \AA}$ are the lattice parameters of the binary compounds.

Assuming a type II-b InAs/InAsSb band offset¹¹ with electrons confined in the InAs layer and holes confined in the InAsSb one, the quantized miniband energies of the strain balanced InAs/InAs_{1-x}Sb_x T2SL were calculated with nextnano3 commercial software¹². At T=150K, for x_{Sb} varying from 0.25 to 0.4 and P varying from 4 nm to 8 nm, cut-off wavelength (λ_{co} or $\lambda_{\text{VH1-C1}}$) corresponding to ground heavy hole VH1 to conduction C1 interminiband energetic transition, is plotted on Fig. 2. For each case, wave functions overlap $|\langle \Psi_{e1} | \Psi_{hh1} \rangle|^2$ values calculated for each fundamental VH1-C1 transition are also specified.

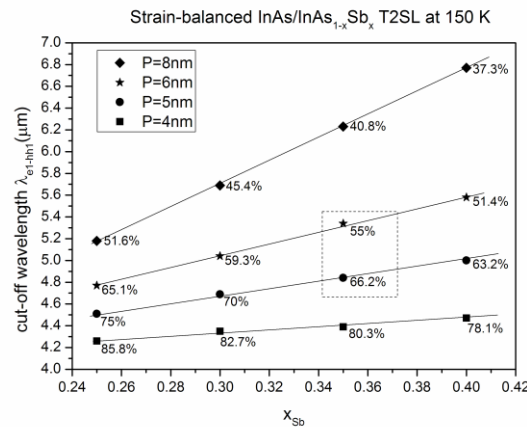


Figure 1. Strain balanced InAs/InAs_{1-x}Sb_x T2SL on GaSb substrate : Calculated cut-off wavelength at T = 150K and associated wave functions overlap of the ground VH1-C1 miniband transition as a function of Sb concentration (x_{Sb}) and for different period thicknesses (P).

3. MBE GROWTH

Ga-free InAs/InAsSb strain balanced SL lattice matched to GaSb have been grown on n-type GaSb Te-doped (100) substrates by solid source MBE equipped with valved crackers set up to produce As₂ and Sb₂ species. Following the thermal oxide desorption, a 400 nm-thick Te-doped GaSb buffer layer was grown before the structure made of a 3 μm thick superlattice region composed of alternating InAs(4.1 nm)/InAsSb(1.4 nm) non intentionally doped (nid) layers and finally capped by a 150 nm-thick n-doped Gasb layer (Fig. 2). Due to the well-known competition for incorporation between Arsenic (As) and Antimony (Sb) in the InAsSb layer, several test samples have been grown to find accurate speed growth of these species leading to lattice-matched structure on GaSb with respect to $x_{\text{Sb}} = 0.35$ in InAsSb layers.

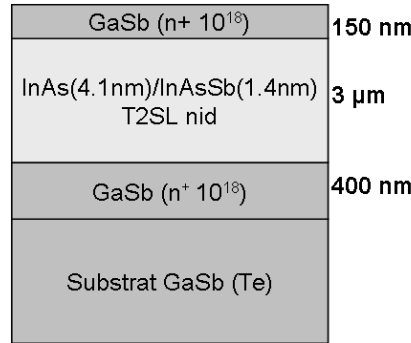


Figure 2. InAs/InAs_{1-x}Sb_x T2SL sample cross-section.

The corresponding high-resolution X-ray diffraction (XRD) spectrum shown in Fig. 3 exhibits many intense satellite peaks with a full-width at half- maximum (FWHM) of the first-order peak (SL0) equals to 44 arcsec, attesting the good crystalline quality of the layers. The targeted SL period value ($P = 5.5\text{nm}$ with layer thicknesses $t_{\text{InAs}} = 4.1\text{ nm}$ and $t_{\text{InAsSb}} = 1.4\text{nm}$ calculated from Eqs (1) and (2) is confirmed by the simulated curve that matches the experimental one.

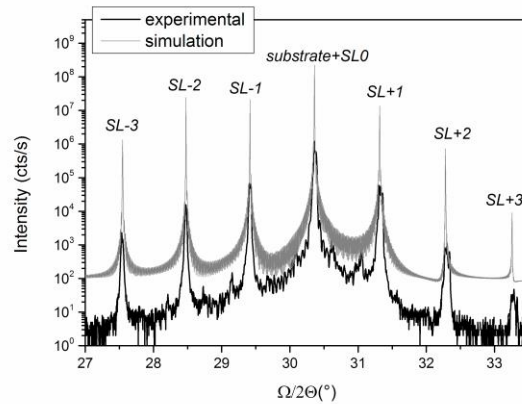


Figure 3. High-resolution XRD spectrum (004) reflection of InAs/InAs_{0.65}Sb_{0.35} T2SL sample ($P = 5.5\text{nm}$) lattice-matched to the GaSb substrate.

In addition, the lattice mismatch calculated using¹³ Eq(3):

$$\frac{\Delta a}{a} = \frac{\sin \theta_{\text{substrate}}}{\sin (\theta_{\text{substrate}} + \Delta \theta)} - 1 \quad (3)$$

where $\theta_{\text{substrate}}$ is the angle in degrees of the substrate peak measured by XRD and $\Delta \theta$ is the angular difference between the substrate peak and the epitaxial peak (the 0th order SL peak in this case) in degrees is less than 300ppm.

The surface morphology has also been observed by atomic force microscopy (AFM) on a $5 \times 5 \mu\text{m}^2$ scan area highlighting well-defined atomic steps (Fig. 4), and measured root-mean-square (RMS) surface roughness only equals to 0.15nm (that is, less than one monolayer in the case of Sb-based materials).

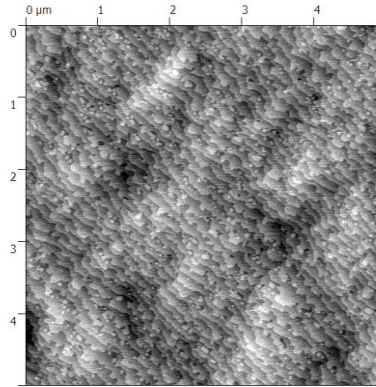


Figure 4. AFM scan of InAs/InAs_{0.65}Sb_{0.35} T2SL sample. Clear monolayer steps can be observed.

4. OPTICAL CHARACTERIZATIONS

The Ga-free InAs/InAsSb SL structure fabricated could be the active zone of a XBn MWIR photodetector. Such a device is designed to be diffusion-current¹ limited. According to Eq. 4, the diffusion-current is inversely proportional to the minority carrier lifetime τ and the carrier concentration N_d :

$$J_d = \frac{q n_i^2}{N_d \tau} L_{diff} \quad (4)$$

Where q is the electrical charge, n_i the intrinsic carrier concentration and L_{diff} the minority carrier diffusion length. As a consequence, determination of τ will give a trend on the expected dark current.

On top of this, it's necessary to ensure that the SL structure is suitable for the full MWIR domain. For this purpose, photoluminescence (PL) measurements allow to reach the bandgap energy of the structure, which will correspond to the 50% cut-off energy of the photodetector spectral response (see section 5.2).

4.1 Photoluminescence

Samples are placed in a cryostat allowing accurate control of the temperature from 10K to 300K and are optically excited with a 50W/cm² power density from a 784nm laser diode modulated at 133kHz through a CaF₂ window. The luminescence signal is analyzed with a Nexus 870 FT-IR system equipped with a MCT detector (12μm cut-off wavelength).

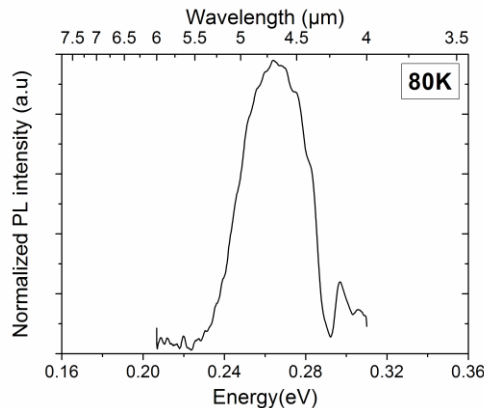


Figure 5. PL spectra at T = 80K of a P = 6nm InAs/InAs_{0.65}Sb_{0.35} SL sample

Fig. 5 shows the normalized PL signal at 80K of a InAs/InAs_{0.65}Sb_{0.35} SL structure with a 6 nm period. The PL peak position, observed at wavelength equal to 4.7μm at 80K, is in agreement with the calculated fundamental valence to conduction interminiband transition (Fig. 1). This result confirms the choice of a T2SL period close to 6nm.

4.2 Photoluminescence decay

To reach the minority carrier lifetime τ , photoluminescence decay (PLD) measurements have been performed on structure presented in Fig. 3. Among contactless techniques, this method remains one of the simplest and most straightforward. The experimental set-up used for PLD measurements is the one described by Delacourt *et al.*¹⁴. Since excess carriers are generated by a pulsed Erbium-doped fiber laser at a wavelength of 1545 nm, it's important to note that, at this wavelength, the light is absorbed by the active layer while the heavily doped buffer and cap layers are transparents. The PLD signals measured at 80K and 150K, for the same level of injection, are reported in Fig. 6. The time-resolved signal is then fitted by a least squares Levenberg–Marquardt method¹⁴ to estimate the contributions from Auger (τ_{Auger}), SRH (τ_{SRH}) and radiative (τ_{rad}) recombinations to the total carrier lifetime, since:

$$\tau = (\tau_{Auger}^{-1} + \tau_{SRH}^{-1} + \tau_{rad}^{-1})^{-1} \quad (5)$$

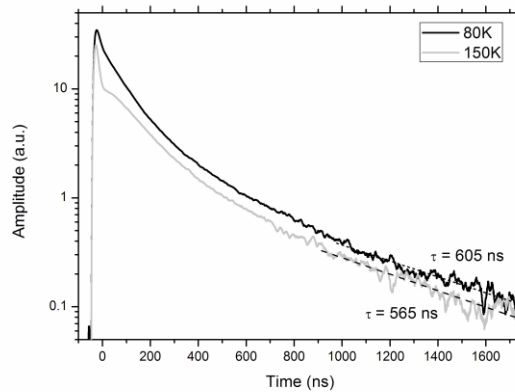


Figure 6. PLD signals of Ga-free sample at T=80K and T=150K.

5. Ga-FREE SL IN XBn CONFIGURATION

The XBn structure is composed of a n-type absorbing layer (AL), an unipolar barrier layer (BL) and a contact layer (CL). The objective of BL is to block majority carrier (electrons) while allowing collection of minority carrier (holes). When properly designed, the use of a wide bandgap BL enables device operation limited by diffusion current¹.

5.1 XBn architecture

The MWIR XBn detector is made of 3 μ m-thick Ga-free InAs/InAs_{0.65}Sb_{0.35} AL, 80nm-thick n-doped AlAs_{0.09}Sb_{0.91} BL and a 150nm-thick n⁺-doped InAs_{0.91}Sb_{0.09} CL (Fig. 7).

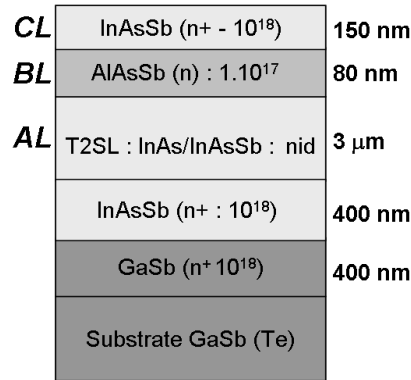


Figure 7. Schematic cross-section of the XBn photodetector.

XRD scan of the complete detector structure is shown in Fig. 8. No angular difference $\Delta\theta \sim 0$ (Eq.3) was detected between the substrate peak and the 0th order AL, indicating lattice-matching of this layer. In contrast, the BL is in compressive strain with a lattice mismatch around 2200ppm and a 94.5% Sb composition in the AlAsSb ternary alloy. Anyway, with a thickness of only 80nm, no relaxation occurs in this layer. In addition, from satellite peak positions (SL-3, SL-2,..., SL+3) we can estimate the period of the AL : P=5.3nm in that case.

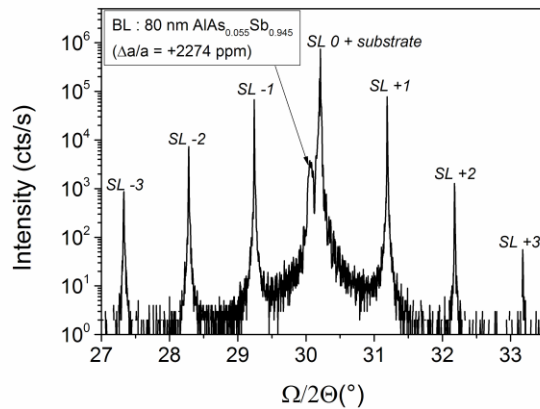


Figure 8. XRD spectrum (004) reflection of the complete XBn structure (P = 5.3nm).

5.2 Experimental results

Standard optical photolithography was used to define detector mesas varying in size from 60 μ m down to 310 μ m in diameter. The mesas were etched down to the GaSb layer with a citric acid/H₂O₂ based etch solution¹⁵. The diodes were passivated by a thin SiO₂ dielectric layer deposited by plasma enhanced chemical vapor deposition (PECVD). Dark current measurements (Fig. 9) as a function of bias and temperature were then conducted under vacuum within a liquid nitrogen cooled Dewar.

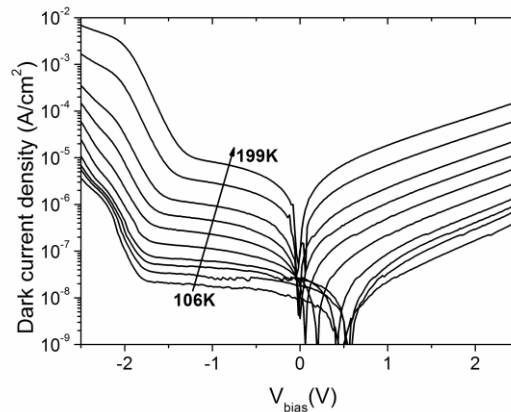


Figure 9. Dark current density vs bias at temperatures between 106K and 199K for a 310µm diameter device.

The Ga-free SL XBn detectors operate under negative bias voltages (negative voltage on the top contact). The bias operation is extracted at -2.5V. This too high value, necessary to allow the transport of holes (minority carriers) from the AL to CL through the BL clearly indicates that the valence band alignment between the BL and AL is not optimized. Normalized spectral response characteristics measured at different temperatures for a 310µm diameter device at bias operation $V_{b}=-2.5V$ are shown in Fig. 10.

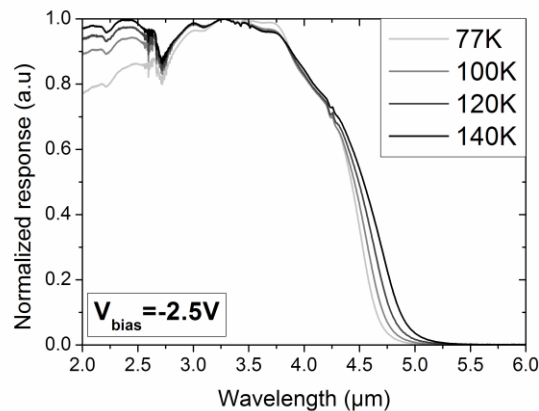


Figure 10. Normalized spectral response measured at different temperatures for a 310µm diameter device at $V_{bias}=-2.5V$.

From these measurements, we extract the cutoff wavelength $\lambda_{co}=4.6\mu m$. This value, a bit lower than the expected one, may probably be explained because of a too short period of the SL (5.3nm obtained vs 5.5 nm targeted).

6. PERFORMANCE COMPARISON

From data presented in Fig. 9, we have plotted on a Arrhenius graph (Fig. 11) the corresponding values of the dark current density at $V_{bias}=-2.5V$ (black circles) as a function of inverse temperature. In addition, to compare the performances of our Ga-free XBn device, we have also plotted in Fig. 11 the data at bias operation of three different types of InSb-based photodetectors¹⁶ (MWIR broadband detectors):

- InSb pn junction fabricated by standard planar process,
- InSb pin junction fabricated by MBE,
- InSb nBn structure fabricated by MBE¹⁷.

The black line in Fig. 11 corresponds to the diffusion regime of XBn structure. Consequently it clearly appears that below 180K, our device is not diffusion limited. Probably, due to its valence band offset with the AL, AlAsSb is not the most appropriate material for the BL. This is evidenced by the large value bias operation we mentioned previously in

section 5.2. As a consequence, the strong bias to be applied on our device to allow holes (minority carriers) collection certainly leads to tunnelling current contribution.

In Fig. 11, the horizontal dashed line indicates the typical photonic current produced in the 3-5 μ m band for f/3 optics by a III-V detector system with a quantum efficiency $\eta = 80\%$ ¹⁸. On top of this, taking into account the criteria according to which a high performance MWIR detector must have a dark current density two decades lower than its photocurrent¹⁹, we also have reported in Fig. 11 the corresponding value (horizontal solid line):

$6 \cdot 10^{-7} \text{ A/cm}^2$.

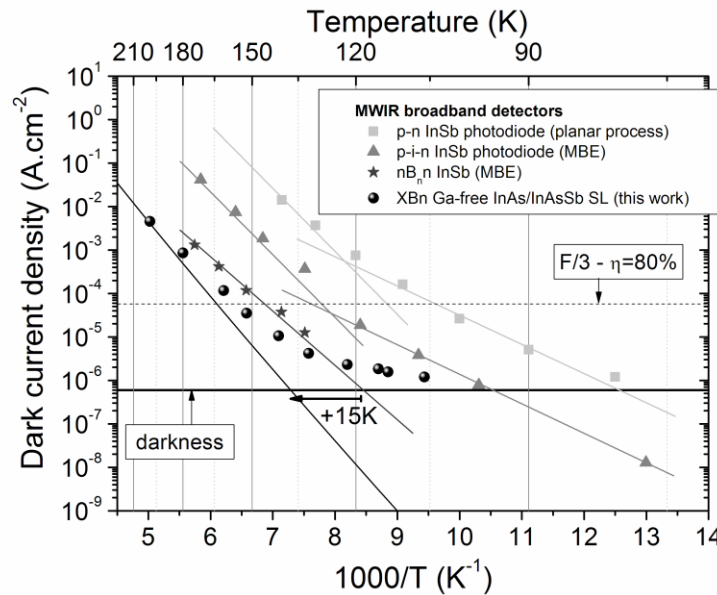


Figure 11. Comparative Arrhenius plot of Ga-free SL with three different types of MWIR broadband InSb-based photodetectors.

Consequently, an optimized Ga-free SL structure in XBn configuration should be able to operate at temperature around 135K-140K, that is, a higher temperature than InSb photodiode's one operating in the full MWIR spectral range.

ACKNOWLEDGEMENTS

Part of this work was supported by the French "Investment for the future" program (Equipex EXTRA ANR11-EQPX-0016).

*jean-philippe.perez@umontpellier.fr

REFERENCES

- [1] P. Klipstein *et al.*, "XBn barrier photodetectors based on InAsSb with high operating temperatures," *Opt Engin.* 50, 061002 (2011).
- [2] A. Manissadjian *et al.*, "Improved IR detectors to swap heavy systems for SWaP," *Proc. SPIE* 8353, 835334 (2012).
- [3] Y. Reibel *et al.*, "Infrared SWAP detectors: pushing the limits," *Proc. SPIE* 9451, 945110 (2015).
- [4] R. Taalat *et al.*, "Influence of the period thickness and composition on the electro-optical properties of type-II InAs/GaSb midwave infrared superlattice photodetectors," *J. Phys. D, Appl. Phys.* 47 015101 (2014).

- [5] S.P. Svensson *et al.*, "Growth of type II strained layer superlattice, bulk InAs and GaSb materials for minority lifetime characterization," J. Cryst. Gr., 334,103 (2011).
- [6] G. Chen *et al.*, "Demonstration of type-II superlattice MWIR minority carrier unipolar imager for high operation temperature application," Opt. Lett. 40, 45 (2015).
- [7] N. Baril *et al.*, "MWIR barrier infrared detectors with greater than 5 μ m cutoff using bulk InAsSb grown on GaSb substrates," Proc. of SPIE Vol. 10177 101771L-1, (2017).
- [8] B.V. Olson *et al.*, "Time-resolved measurements of minority carrier recombination in a mid-wave infrared InAsSb alloy and InAs/InAsSb superlattice," Appl. Phys. Lett. 101, 092109 (2012).
- [9] A. Haddadi *et al.*, "Bias selectable dual-band mid-/long-wavelength infrared photodetectors based on InAs/InAs_{1-x}Sb_x type-II superlattices," Appl. Phys. Lett. 106, 011104 (2015).
- [10] D.R. Rhiger *et al.*, "Analysis of III-V superlattice nBn device characteristics," J. Electron. Mater. 45, 4646 (2016).
- [11] D. Lackner *et al.*, "InAs/InAsSb strain balanced superlattices for optical detectors: Material properties and energy band simulations," J. Appl. Phys. 111, 034507 (2012).
- [12] <http://www.nextnano.de/nextnano3/> for more information about the nextnano3 software.
- [13] T. Schuler-Sandy *et al.*, "Growth of InAs-InAsSb SLS through the use of digital alloys," J. Cryst. Gr., 425, 29 (2015).
- [14] B. Delacourt *et al.*, "Temperature and Injection Dependence of Photoluminescence Decay in Midwave Infrared HgCdTe," J. Elec.Mat., 46, 12 (2017).
- [15] O. Dier *et al.*, "Selective and non-selective wet chemical etchants for GaSb-based materials," Semicond. Sci. Technol., 19, 1250-1253 (2004).
- [16] J. P. Perez *et al.*, "MWIR InSb detector with nBn architecture for high operating temperature," Proc. SPIE 9370 93700N-93700N-7 (2015)
- [17] A. Evirgen *et al.*, "Midwave infrared InSb nBn detector," Elec. Lett., 50, 20, 1472-1473 (2014)
- [18] M. A. Kinch *et al.*, "High Operating temperature MWIR detectors," Proc. of SPIE, 7660, 76602V-1 (2010).
- [19] P. C. Klipstein *et al.*, "Third-generation infrared detector program at SCD," Proc. of SPIE, 5406, 222-229 (2004).